Effects of surface proximity and force orientation on the feeding flows of microorganisms on solid surfaces

Mads Rode ⬤,[1,*] Giulia Meucci,[1,2] Kristian Seegert,[1]
Thomas Kiørboe ⬤,[3] and Anders Andersen ⬤[1,*,†]

[1]*Department of Physics and Centre for Ocean Life, Technical University of Denmark,
DK-2800 Kgs. Lyngby, Denmark*
[2]*Politecnico di Milano, IT-20133 Milan, Italy*
[3]*Centre for Ocean Life, National Institute of Aquatic Resources, Technical University of Denmark,
DK-2800 Kgs. Lyngby, Denmark*

Many aquatic microorganisms are attached to solid surfaces while creating feeding flows that bring prey particles to them. To explore the effects of surface proximity and orientation of the flow-generating force, we analyze the low-Reynolds-number flow due to a point force above a plane no-slip surface. The presence of the surface reduces the feeding flow relative to the unbounded situation. We show that the reduction of the flow rate through a circular clearance disk perpendicular to the force and centered at its position is twice as large when the force is perpendicular to the surface as when it is parallel. When the force is perpendicular to the surface, the flow forms a toroidal eddy with closed streamlines, and the resulting flow recirculation may lead to refiltration of water that has already been cleared for prey. We prove that due to the nature of the far-field flow, the shortest recirculation time along a streamline through a circular clearance disk is inversely proportional to the flow rate to the power four. Finally, we discuss the biological advantages and disadvantages of perpendicular and parallel force orientation and the effects of prey diffusion and ambient flow, and we argue that recirculation is irrelevant in the typical perpendicular feeding flow since the recirculation time is long compared to the biologically relevant timescales.

I. INTRODUCTION

Many aquatic microorganisms are suspension feeders that use flagella or cilia to generate feeding flows through clearance zones where they retain suspended prey particles. Flagellates and ciliates commonly attach to surfaces of aquatic plants, larger organisms, and millimeter-sized aggregations of smaller particles known as marine snow (Fig. 1). Sessile flagellates such as the choanoflagellate *Salpingoeca rosetta* and ciliates like *Vorticella convallaria* attach to solid surfaces with a stalk and generate a feeding flow either away from or toward the surface [1–12]. Other species of ciliates such as *Cyclidium glaucoma* and *Euplotes vannus* sit on solid surfaces while generating a feeding flow parallel to the surface [4,5]. How is the foraging of such organisms and in particular the clearance rate, i.e., the flow rate through the clearance zone, affected by the proximity to the surface and the orientation of the flow-generating force?

In the vast open water masses of the oceans, marine snow is the most important source of habitats for attached suspension feeders, and we therefore consider marine snow as our primary biological

---

*Present address: Centre for Ocean Life, National Institute of Aquatic Resources, Technical University of Denmark, DK-2800 Kgs. Lyngby, Denmark.

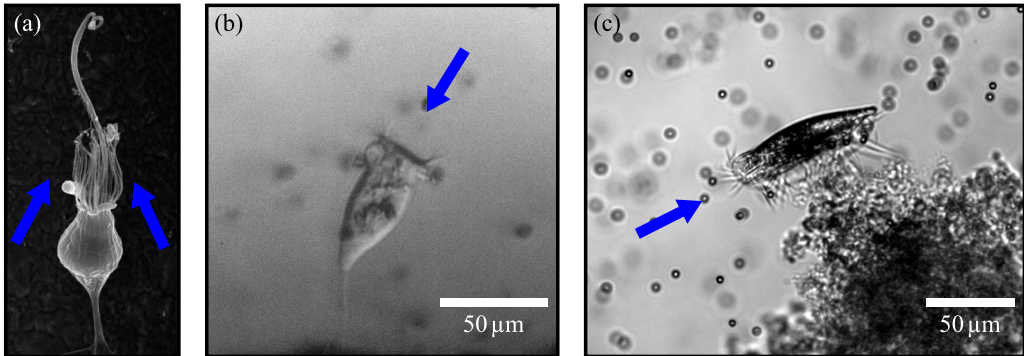†Corresponding author: aanders@aqua.dtu.dk

FIG. 1. Examples of suspension feeding microorganisms on solid surfaces. (a) The choanoflagellate *S. rosetta* (scanning electron micrograph courtesy of Mark J. Dayel) [13], (b) the ciliate *V. convallaria* (image courtesy of Rachel E. Pepper), and (c) the ciliate *E. vannus* sitting on a lump of organic material. The equivalent spherical radius of the cell of *S. rosetta* is typically 2 μm. The blue arrows indicate the flow directions. The choanoflagellate *S. rosetta* and the ciliate *V. convallaria* generate feeding flows away from and toward the surface, respectively, and the ciliate *E. vannus* generates a feeding flow roughly parallel to the surface.

example. Marine snow forms microbial hot spots, and feeding in this environment is favorable for suspension feeders that feed on bacteria and small flagellates [14–17]. Prey come from two sources: (1) chemotactic microorganisms that are attracted toward the surface by leaking, dissolved organic material [15,18] and (2) microorganisms that leave the productive biofilm on the surface [19–21]. The incoming flux density to a spherical collector is proportional to the product of the ambient concentration and the diffusion coefficient of the motile prey and inversely proportional to the radius of the marine snow particle [22], whereas the flux density of detaching motile prey is proportional to the density and the detachment rate of attached prey on the surface. Densities of bacterial and flagellate prey attached to marine snow are many orders of magnitude higher than in the ambient water [19,20], and the residence time, i.e., the time that prey spend at the surface, can be short, on the order of a few hours [21]. Attached suspension feeders positioned above competitors that are directly on the surface may enjoy a competitive advantage by removing incoming prey before it reaches the surface. Conversely, suspension feeders positioned near the surface may benefit from the high concentration of microorganisms in the immediate vicinity of the surface.

To explore the fluid dynamical effects of surface proximity and force orientation, we consider the solution derived by Blake and coworkers for the steady flow at low Reynolds number due to a point force above a plane no-slip surface [23–27]. Fenchel used the solution to model feeding flows of attached suspension feeders, and he showed that the proximity to the surface reduces the clearance rate more strongly in the perpendicular than in the parallel case [5]. Here we derive analytic clearance rate expressions in both situations, and we quantify the comparison. When the force is perpendicular to the surface, the flow forms a toroidal eddy as observed in feeding flows of choanoflagellates and ciliates [1,2,8], and the resulting flow recirculation may lead to refiltration of water that has already been cleared for prey [3,5,6,9]. Sessile microorganisms like *V. convallaria* can vary their orientation and height above the surface with time [2,9], and periodic variation of the vertical position of the force disrupts the steady toroidal eddy as shown using the so-called blinking Stokeslet model [6]. However, even in a steady, perpendicular feeding flow, refiltration is only an issue if the recirculation time is short compared to the timescales for prey transport by Brownian motion, self-motility, and ambient flow. Here, we shall determine the recirculation times analytically and address the significance of refiltration.

In the following, we first summarize the flow solution derived by Blake and coworkers [23–25]. Building on the solution we derive analytic expressions for the flow rate through a circular clearance disk that is centered at the position of the force and oriented perpendicular to it, both when the force

is perpendicular and when it is parallel to the surface. When the force is perpendicular to the surface, we also obtain the clearance rate when the center of the circular clearance disk is displaced up or down relative to the position of the force. When the force is parallel to the surface, we explore how well the optimal clearance zones can be approximated by circular clearance disks. Furthermore, we determine the recirculation times of the flow along the closed streamlines when the force is perpendicular to the surface. Finally, we discuss the biological implications of our theoretical findings.

II. POINT FORCE MODEL

We model the feeding flow as the low-Reynolds-number flow due to a point force, $\boldsymbol{F}$, that acts at the point $\boldsymbol{X} = (0, 0, h)$ in the infinite half-space above a solid surface represented by the xy plane at which we apply the no-slip boundary condition. The governing equations are the time-independent Stokes equations for Newtonian and incompressible flow:

$$-\boldsymbol{\nabla} p + \mu \nabla^2 \boldsymbol{v} = \boldsymbol{0}, \quad \boldsymbol{\nabla} \cdot \boldsymbol{v} = 0, \tag{1}$$

where p denotes the pressure field, $\boldsymbol{v}$ the velocity field, and μ the viscosity. The solution can be written in the compact form [23,24]:

$$v_i = \frac{F_j}{8\pi\mu} \left\{ \frac{\delta_{ij}}{|\boldsymbol{x} - \boldsymbol{X}|} + \frac{(x_i - X_i)(x_j - X_j)}{|\boldsymbol{x} - \boldsymbol{X}|^3} - \frac{\delta_{ij}}{|\boldsymbol{x} - \boldsymbol{X}^*|} - \frac{(x_i - X_i^*)(x_j - X_j^*)}{|\boldsymbol{x} - \boldsymbol{X}^*|^3} \right.$$

$$\left. + 2h(\delta_{j\alpha}\delta_{\alpha k} - \delta_{j3}\delta_{3k}) \frac{\partial}{\partial x_k} \left[\frac{h(x_i - X_i^*)}{|\boldsymbol{x} - \boldsymbol{X}^*|^3} - \frac{\delta_{i3}}{|\boldsymbol{x} - \boldsymbol{X}^*|} - \frac{(x_i - X_i^*)(x_3 - X_3^*)}{|\boldsymbol{x} - \boldsymbol{X}^*|^3} \right] \right\}, \tag{2}$$

$$p = \frac{F_j}{4\pi} \left[\frac{x_j - X_j}{|\boldsymbol{x} - \boldsymbol{X}|^3} - \frac{x_j - X_j^*}{|\boldsymbol{x} - \boldsymbol{X}^*|^3} - 2h(\delta_{j\alpha}\delta_{\alpha k} - \delta_{j3}\delta_{3k}) \frac{\partial}{\partial x_k} \frac{x_3 - X_3^*}{|\boldsymbol{x} - \boldsymbol{X}^*|^3} \right], \tag{3}$$

where $\boldsymbol{x} = (x, y, z)$ is the field point, $\boldsymbol{X}^* = (0, 0, -h)$ the image point, and $\alpha = 1, 2$. The term $\delta_{j\alpha}\delta_{\alpha k} - \delta_{j3}\delta_{3k}$ is equal to 1 if $j = k = 1, 2$ and -1 if $j = k = 3$. The force may point in any direction, but we focus our attention on the two generic cases in which it is either perpendicular or parallel to the surface.

The flow in the perpendicular case has rotational symmetry around the z axis, and the velocity components can be expressed as partial derivatives of a Stokes stream function. In cylindrical polar coordinates the velocity components become:

$$v_s = \frac{1}{s} \frac{\partial \Psi}{\partial z}, \quad v_z = -\frac{1}{s} \frac{\partial \Psi}{\partial s}, \tag{4}$$

where $s = \sqrt{x^2 + y^2}$ is the radial coordinate. The stream function, Ψ, can be written:

$$\Psi(s, z) = \frac{F s^2}{8\pi\mu} \left\{ \frac{1}{\sqrt{s^2 + (z - h)^2}} - \frac{1}{\sqrt{s^2 + (z + h)^2}} - \frac{2hz}{[s^2 + (z + h)^2]^{3/2}} \right\}, \tag{5}$$

where we have assumed that the force is pointing toward the surface [6,25]. This choice models sessile ciliates such as *V. convallaria*, whereas the flow-generating force of sessile choanoflagellates like *S. rosetta* points away from the surface and leads to an identical streamline pattern with reversed flow direction [5].

The height of the point force above the wall, h, provides the characteristic length scale, and we can define characteristic scales for time, flow speed, and stream function:

$$T_0 = \frac{8\pi\mu h^2}{F}, \quad v_0 = \frac{F}{8\pi\mu h}, \quad \Psi_0 = \frac{F h}{8\pi\mu}. \tag{6}$$

In the following we shall use the characteristic scales throughout our analysis and plots.
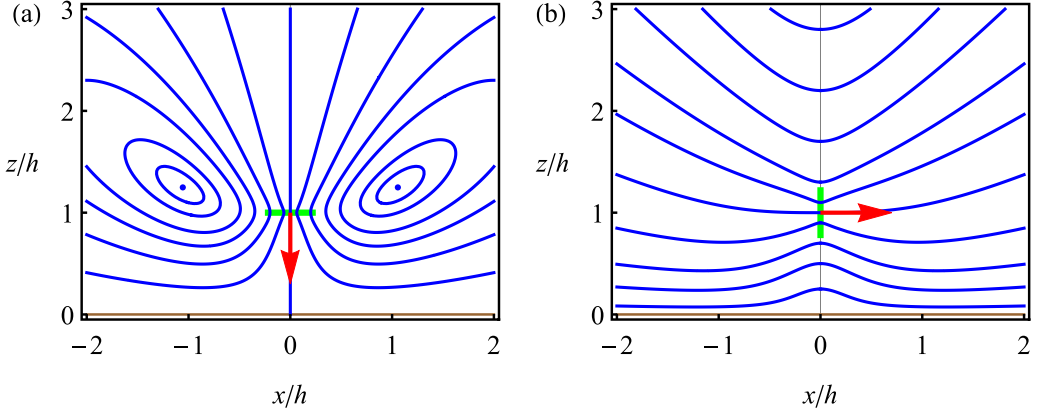
FIG. 2. Streamlines and clearance zones in the point force model. The point force (red arrow) is placed at the height h above the plane no-slip surface, and it is oriented respectively (a) perpendicular and (b) parallel to the surface. Both plots show a circular clearance disk (green) that is centered at the position of the point force and oriented perpendicular to it.

III. EFFECTS OF SURFACE PROXIMITY AND FORCE ORIENTATION

The streamlines are closed and the flow forms a toroidal eddy when the force is perpendicular to the surface [27], whereas there are no closed streamlines and the velocity component in the direction of the force is positive when the force is parallel to the surface (Fig. 2). In the perpendicular case we obtained the streamlines as contour lines of the stream function, and in the parallel case we determined them by numerical integration since a streamfunction does not exist. In the perpendicular case the stream function is zero on the axis of symmetry, $\Psi(0, z) = 0$, and its maximum value, $\Psi_{max} = 0.3974\Psi_0$, is found at the center of the toroidal eddy which has the coordinates $s_{max} = 1.0565h$ and $z_{max} = 1.2482h$ [25].

In the perpendicular case, the flow rate, Q, through a circular clearance disk centered on the axis of symmetry and oriented perpendicular to it is proportional to the stream function evaluated at the rim of the disk:

$$Q = -2\pi \int_0^a v_z(s, d)s \, ds = 2\pi \Psi(a, d), \tag{7}$$

where a is the radius of the disk and d its height above the wall [28]. Using the stream function in Eq. (5) we therefore readily obtain the general clearance rate expression:

$$Q = \frac{Fa^2}{4\mu} \left\{ \frac{1}{\sqrt{a^2 + (d-h)^2}} - \frac{1}{\sqrt{a^2 + (d+h)^2}} - \frac{2hd}{[a^2 + (d+h)^2]^{3/2}} \right\}. \tag{8}$$

The maximum value of the clearance rate is obtained when the rim of the clearance disk coincides with the center of the toroidal eddy:

$$Q_{max} = 2\pi \Psi_{max} = 0.3121 \frac{Fh}{\pi\mu} = 2.4968\Psi_0. \tag{9}$$

Fenchel derived by integration the flow rate through a circular clearance disk at the same height as the force [5]. By setting $d = h$ in Eq. (8) we obtain Fenchel's formula:

$$Q = \frac{Fa}{4\mu} \left[1 - \frac{a}{\sqrt{a^2 + 4h^2}} - \frac{2ah^2}{(a^2 + 4h^2)^{3/2}} \right], \tag{10}$$
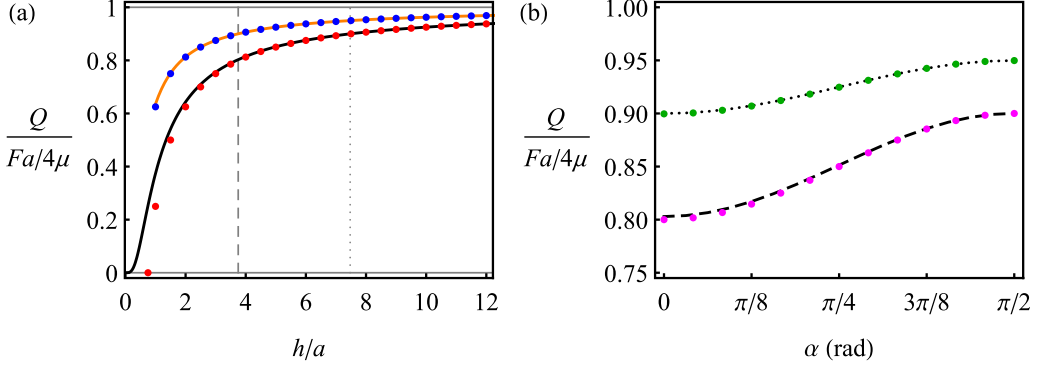
FIG. 3. Clearance rates for different force orientations. (a) The complete expression (10) for the perpendicular case (black solid line), the approximation (11) for the perpendicular case (red dots), the complete expression for the parallel case evaluated numerically (orange solid line), and the approximation (13) for the parallel case (blue dots). The clearance rate is equal to 90% of the clearance rate for the Stokeslet in the unbounded domain when $h/a = 3.8$ in the parallel case (gray dashed line) and $h/a = 7.5$ in the perpendicular case (gray dotted line). (b) The clearance rate as function of the angle between the force and the inward surface normal when $h/a = 3.8$ (black dashed line) and (magenta dots) and $h/a = 7.5$ (black dotted line) and (green dots). The complete expressions are shown as lines and the approximations (14) as dots.

where the prefactor $Fa/(4\mu)$ is the flow rate for the corresponding Stokeslet in the unbounded domain [5]. The flow rate for a Stokeslet in an unbounded domain is the maximum that an attached microorganism can possibly attain, and the presence of the no-slip surface reduces the flow rate relative to the unbounded situation. When $d = h$ and $a \ll h$ we may approximate the flow rate by the Taylor series:

$$Q \approx \frac{Fa}{4\mu}\left(1 - \frac{3a}{4h}\right), \tag{11}$$

which we shall compare below with the corresponding approximation in the parallel case.

In the parallel case, we again focus on the flow rate through a circular clearance disk that is centered at the position of the force and oriented perpendicular to it [Fig. 2(b)]. We note that the flow rate is defined only when $a \leqslant h$ due to the geometry of the problem [5]. To determine the flow rate we write the velocity component v_x in the yz plane using polar coordinates $y = q \cos\phi$ and $z = h + q \sin\phi$. Building on Eq. (2) we find:

$$v_x = \frac{F}{8\pi\mu}\left[\frac{1}{q} - \frac{1}{\sqrt{q^2 + 4hq\sin\phi + 4h^2}} - \frac{2h(h + q\sin\phi)}{(q^2 + 4hq\sin\phi + 4h^2)^{3/2}}\right]$$

$$\approx \frac{F}{8\pi\mu}\left(\frac{1}{q} - \frac{3}{4h} + \frac{3q\sin\phi}{8h^2}\right), \tag{12}$$

where we have assumed that $q \ll h$ to obtain the Taylor series. By integrating the approximate expression for v_x over the clearance disk, we obtain the flow rate approximation:

$$Q \approx \frac{F}{8\mu\pi}\int_0^a \int_0^{2\pi}\left(\frac{1}{q} - \frac{3}{4h} + \frac{3q\sin\phi}{8h^2}\right)q\,dq\,d\phi = \frac{Fa}{4\mu}\left(1 - \frac{3a}{8h}\right). \tag{13}$$

The second-order term in the approximation of v_x does not contribute to the flow rate, since it vanishes in the integration due to its angular dependence.

The flow rate in the perpendicular case is reduced more strongly due to the proximity of the surface than in the parallel case [Fig. 3(a)]. The approximation in the perpendicular case (11) captures the complete expression well with less than 3% deviation when $h > 2a$. The approximation

in the parallel case (13) agrees well with the complete expression in the entire range $h > a$ with less than 2% deviation, since the second-order term does not contribute to the flow rate. We see that when $h > 2a$ the reduction of the flow rate due to the surface is twice as large in the perpendicular case compared to the parallel case. The ratios $h/a = 3.8$ and $h/a = 7.5$ with parallel and perpendicular force orientation, respectively, correspond to 90% of the clearance rate for the Stokeslet in the unbounded domain [Fig. 3(a)], and such ratios are typical for suspension feeders in nature ([5], Table 2). The approximations (11) and (13) are special cases of the general approximation for the flow rate through a circular clearance disk perpendicular to the force and centered at its position:

$$Q \approx \frac{Fa}{4\mu}\left[1 - \frac{3(1 + \cos^2 \alpha)a}{8h}\right], \tag{14}$$

where α denotes the angle between the force and the inward surface normal. To derive the approximation we estimated the reduction of the flow rate due to the image system by evaluating its contribution to the velocity component in the direction of the force at the position of the force and multiplying it by the area of the clearance disk. The approximation increases monotonically from the minimum value in the perpendicular case ($\alpha = 0$) to the maximum value in the parallel case ($\alpha = \pi/2$), and it agrees well with the numerically evaluated complete expression when $h/a = 3.8$ and $h/a = 7.5$ [Fig. 3(b)].

IV. OPTIMAL CLEARANCE ZONES IN THE PARALLEL CASE

In the perpendicular case the flow has rotational symmetry and circular clearance disks are optimal, i.e., for a given disk area the flow rate is maximum through a clearance disk with circular shape that is centered at the position of the force [5]. The optimal clearance disks in the parallel case need not be circular as implicitly assumed above, and we shall therefore explore how well they can be approximated by circular clearance disks.

The contour lines of v_x form the boundaries of the optimal clearance disks in the yz plane. This result follows if we imagine perturbing a clearance disk bounded by a contour line while keeping its area constant. Any such perturbation will lower the clearance rate, since it will lead to a clearance disk that includes a "new" region with low values of v_x while excluding an "old" region with high values of v_x. In the vicinity of the force, the contour lines labeled by the numbers $k = v_x/v_0$ are approximately circles centered at the position of the force, and further away they appear flattened and centered above the position of the force [Fig. 4(a)]. The flow rate, Q, increases at decreasing rate with the effective radius, b, of the optimal clearance disk, i.e., the radius of the circular disk with the same area as the optimal clearance disk [Fig. 4(b)]. The flow rates are shown normalized by the total flow rate in the direction of the force as determined by Liron [26]:

$$Q_{\text{tot}} = \int_{-\infty}^{\infty}\int_{0}^{\infty} v_x(0, y, z)dydz = \frac{Fh}{\pi\mu} = 8\Psi_0. \tag{15}$$

Ciliates with parallel feeding flows typically have h/b in the range 3–4 [5], corresponding to k in the range 2.3–3.3 and $Q/Q_{\text{tot}} = 0.18$–0.23 [Fig. 4(b)]. We therefore see that the model in biologically relevant situations predicts that the optimal clearance disks are close to circular and carry significant fractions of the total flow rate through the entire half-plane.

V. RECIRCULATION TIME IN THE PERPENDICULAR CASE

When the force is perpendicular to the surface, the recirculation time along a given closed streamline in the toroidal eddy can be determined numerically by solving the coupled first-order differential equations for the streamline. From an initial point we integrate forward in time while monitoring the distance to the initial point. When returning to the vicinity of the initial point, we integrate with refined time steps until we pass the initial point and the distance increases again. The recirculation time is long for the streamlines that pass close to the force and short for the
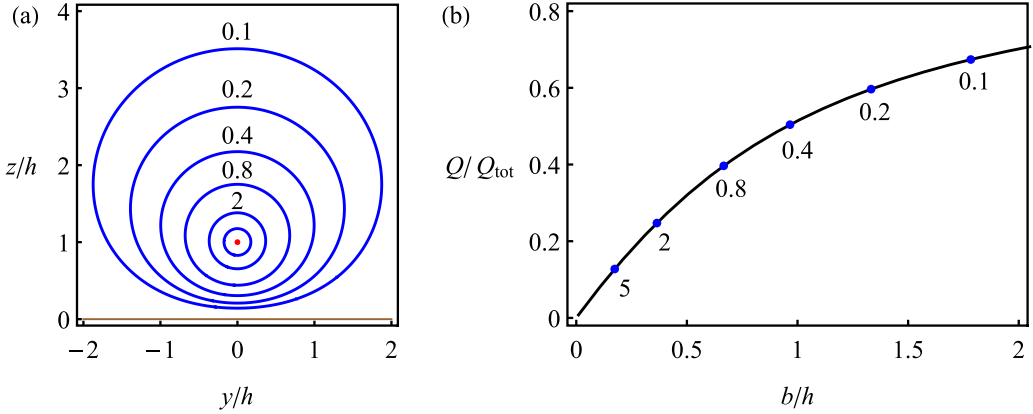
FIG. 4. Optimal clearance zones and clearance rates when the force is parallel to the surface. (a) The boundaries of the optimal clearance disks are contour lines of v_x (blue solid lines), and the position of the force is indicated by the red dot. (b) The flow rate, Q, for the optimal clearance disks as function of the effective radius of the clearance disk, b. The flow rate is normalized by the total flow rate defined in Eq. (15). The contour lines in (a) correspond to the points (blue dots) in (b), and the numbers indicate the values of $k = v_x/v_0$, where v_0 is defined in Eq. (6).

streamlines near the center of the toroidal eddy [Fig. 5(a)]. The recirculation time varies by three orders of magnitude for the selected streamlines, and we find that it is inversely proportional to the stream function to the power four [Fig. 5(b)]. Pepper and coworkers numerically determined a similar power law for the recirculation time as function of the radial coordinate, s, for the streamlines that cross $z = h$ [9]. The two power laws are related since $\Psi/\Psi_0 \approx s/h$ when $z = h$ and $s \ll h$.

The streamlines that come close to the z axis return far away from the force where the flow speed is low and therefore determining for the long recirculation times. To understand the dependence of the recirculation time on the stream function, we shall therefore consider the far field flow. The flow
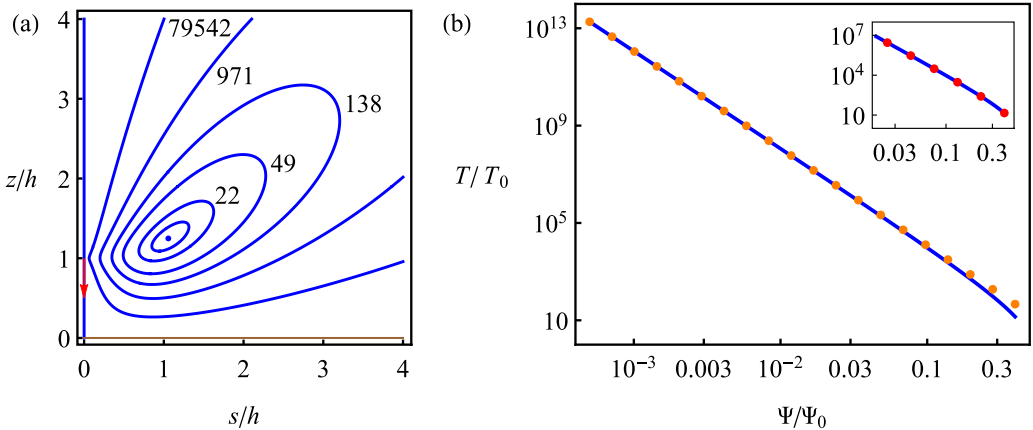

FIG. 5. Recirculation times along the closed streamlines when the force is perpendicular to the wall. (a) The numerically determined recirculation times are shown for selected streamlines in units of the timescale T_0. (b) The recirculation time, T, as function of the stream function, Ψ, normalized by T_0 and Ψ_0, respectively. Numerical results for the complete flow solution (blue solid line) and the analytically determined power law in Eq. (23) (orange dots). The inset shows the numerical results for the complete flow solution (blue solid line) and the analytic approximation in Eq. (24) (red dots).

speed decreases as one over distance cubed in the far field when the force is perpendicular to wall [24], and we have the velocity components:

$$v_s = \frac{F}{8\pi\mu} \frac{6h^2sz(2s^2 - 3z^2)}{(s^2 + z^2)^{7/2}}, \tag{16}$$

$$v_z = \frac{F}{8\pi\mu} \frac{6h^2z^2(3s^2 - 2z^2)}{(s^2 + z^2)^{7/2}}. \tag{17}$$

The corresponding approximation of the stream function decreases as one over distance:

$$\Psi = \frac{6\Psi_0 hs^2z^2}{(s^2 + z^2)^{5/2}}, \tag{18}$$

and in polar coordinates r and θ it reads:

$$\Psi = \frac{6\Psi_0 h \sin^2\theta \cos^2\theta}{r} = \frac{3\Psi_0 h(1 - \cos 4\theta)}{4r}, \tag{19}$$

where $s = r\cos\theta$ and $z = r\sin\theta$. Since the streamlines are contour lines of the stream function, we can readily obtain the polar representation of the streamlines:

$$r = \frac{3\Psi_0 h}{4\Psi}(1 - \cos 4\theta). \tag{20}$$

The shape of the approximate streamlines is related to the shape of the cardioid curve [29], i.e., the curve shapes are similar except that the arguments of the parametric representations differ by a factor of four. A complete loop corresponds to going from $\theta = 0$ to $\theta = \pi/2$, and the recirculation time can therefore be obtained from the angular velocity. Using Eqs. (16) and (17) we find the radial velocity:

$$\frac{dr}{dt} = \frac{12\Psi_0 h \cos 2\theta \sin\theta}{r^3}, \tag{21}$$

and by applying Eq. (20) we obtain the angular velocity:

$$\frac{d\theta}{dt} = \frac{\Psi}{3\Psi_0 h \sin 4\theta} \frac{dr}{dt} = \frac{\Psi^4}{216\Psi_0^4 T_0 \sin^6\theta \cos^7\theta}. \tag{22}$$

We rearrange the expression, and by integration we find that the recirculation time is inversely proportional to the stream function to the power four:

$$\frac{T}{T_0} \approx \frac{216\Psi_0^4}{\Psi^4} \int_0^{\pi/2} \sin^6\theta \cos^7\theta \, d\theta = \frac{1152\Psi_0^4}{1001\Psi^4}. \tag{23}$$

The analytically determined power law for the recirculation time as function of the stream function agrees well with the numerical result [Fig. 5(b)]. However, to fully capture the numerical result, we need to include the next to leading-order term in the far field approximation. Following the procedure outlined above, we obtain the recirculation time:

$$\frac{T}{T_0} \approx \frac{1152\Psi_0^4}{1001\Psi^4} - 2\frac{\Psi_0^3}{\Psi^3}. \tag{24}$$

The expression agrees quantitatively with the numerical result, and it captures the deviation from the power law near the center of the toroidal eddy [Fig. 5(b), inset].

The recirculation time approaches a limiting value, $T_{\min}$, as the center of the toroidal eddy is approached. To determine $T_{\min}$ we apply concepts from dynamical systems theory and consider the eigenvalues of the Jacobian matrix evaluated at the center of the eddy:

$$\mathbf{J} = \begin{pmatrix} \partial_s v_s & \partial_z v_s \\ \partial_s v_z & \partial_z v_z \end{pmatrix}\bigg|_{s=s_{\max}, \, z=z_{\max}}. \tag{25}$$

The pair of purely imaginary eigenvalues are related to the limiting value of the recirculation time via $\lambda_\pm = \pm i 2\pi / T_{min}$ [30]. To determine the eigenvalues, we use Eq. (4) to express the velocity components in terms of the stream function in Eq. (5), and we find the limiting value of the recirculation time:

$$T_{min} = \left. \frac{2\pi s}{\sqrt{(\partial_s^2 \Psi)(\partial_z^2 \Psi) - (\partial_s \partial_z \Psi)^2}} \right|_{s=s_{max},\ z=z_{max}} = 14.0370\, T_0. \qquad (26)$$

The theoretically determined value agrees well with the value obtained by direct numerical integration of the coupled first-order differential equations [Fig. 5(b)].

VI. DISCUSSION

In the perpendicular case, we derived the general clearance rate expression in Eq. (8) for the situation in which the point force and the clearance disk are positioned at different heights above the surface. The expression has practical applicability, since flow generation and prey interception takes place at different heights for some microorganisms (Fig. 1). Sessile ciliates such as *V. convallaria* use their cilia bands to both create the feeding flow and intercept prey particles [2,4], but sessile choanoflagellates such as *S. rosetta* generate the feeding flow with their flagellum and intercept prey particles on their collar filter closer to the surface [1,5]. Furthermore, for attached microorganisms that create a flow toward the surface it may be advantageous to determine the clearance rate through an imaginary clearance disk positioned some distance above the organism where the simplifying assumptions of the point force model are more fully justified.

Parallel feeders do not need to be positioned very high above the surface to achieve the same flow rate as organisms with perpendicular feeding flow. The ratios $h/a = 3.8$ for parallel feeders and $h/a = 7.5$ for perpendicular feeders are typical for flagellates and ciliates in nature [5], and the model predicts that the ratios correspond to 90% of the maximum clearance rate that an attached microorganism can possibly attain [Fig. 3(a)]. For organisms attached to marine snow particles, we conjecture that parallel feeders may in particular feed on the prey that leave the surface, whereas stalked, perpendicular feeders that harvest prey relatively far from the surface may preferentially remove incoming prey before it reaches the surface and the parallel feeders. Depending on the concrete situation, the flux density of prey that leave the surface may be smaller, similar to, or higher than the incoming flux density, thus favoring one or the other foraging strategy. When attached to a plane surface, suspension feeders are typically not creating their feeding flow exactly perpendicular or parallel to the surface, and surfaces of marine snow particles and other habitats for attached suspension feeders are often rough at the length scale of the organism (Fig. 1). However, the general clearance rate approximation in Eq. (14) suggests that our main conclusions are robust [Fig. 3(b)].

When the force is perpendicular to the surface, we showed that the long recirculation time and its dependence on the stream function is a result of the one over distance cubed decrease of the flow speed in the far field (Fig. 5). We can link the recirculation times determined from the far field behavior to the clearance rates and the radii of the circular clearance disks in the vicinity of the force using Eq. (7). The clearance rate increases with the radius of the disk, but at a decreasing rate when $a > 0.21h$, i.e., the increase comes with diminishing returns [Fig. 6(a)]. This feature is further emphasized by the increase of the risk of refiltration due to the decrease of the shortest recirculation time the disk [Fig. 6(b)], an effect that has already been pointed out by Pepper and coworkers [9]. However, perpendicular feeders in nature are observed to have $a \leqslant 0.2h$ [5], and if we as an example consider a sessile microorganism with $a = 0.2h$ and $T_0 = 0.5$–5 s (Table I), we find $Q = 0.25 Q_{max}$ and $T = 9.9 \times 10^3 T_0 = 1$–14 h, i.e., the clearance rate is 25% of the maximum possible value and the shortest recirculation time is between 1 h and half a day. The recirculation time is therefore long compared with the biologically relevant timescales, such as the timescales for active variation of orientation and height above the surface.
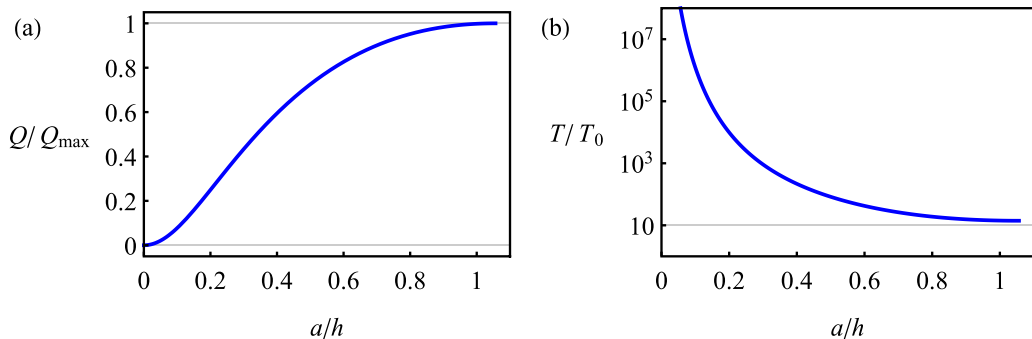
FIG. 6. The flow rate, Q, through a circular clearance disk and the shortest recirculation time, T, along a streamline through the disk as functions of the radius of the disk, a, when the force is perpendicular to the surface. The clearance disk is positioned at the height $d = z_{max}$ above the surface corresponding to the height of the center of the toroidal eddy. (a) The flow rate in Eq. (8) is normalized by the maximum flow rate, Q_{max}, determined in Eq. (9), and (b) the numerically determined recirculation time is normalized by the timescale T_0.

Nonmotile bacteria display Brownian motion, and motile bacteria and small flagellates move with run-tumble motion. Prey are therefore not passive tracers that perfectly follow the streamlines of the feeding flow. The motion of motile prey can be treated as diffusive when the run length is short compared with the size of the clearance zone whereas it should be treated as ballistic when the run length is long [31]. To describe the relative importance of advection and diffusion in the feeding flow toward the clearance zone, we consider the Péclet number: $\mathrm{Pe} = h v_0 / D$, where v_0 is the characteristic flow speed defined in Eq. (6) and D the diffusion coefficient [9]. Typical values of diffusion coefficients are $D = 0.2 \ \mu\mathrm{m}^2 \, \mathrm{s}^{-1}$ for nonmotile, bacteria-sized prey and $D = 30 \ \mu\mathrm{m}^2 \mathrm{s}^{-1}$ for motile, bacterial prey [31–33]. With $F = 50$–500 pN and $\mu = 1 \times 10^{-3}$ Pa s (Table I), we find $\mathrm{Pe} = 10^4$–10^5 for nonmotile prey and $\mathrm{Pe} = 10^2$–10^3 for motile prey, indicating that the prey transport toward the clearance zone is advectively dominated. The time, T_D, that it takes for a prey organism to diffuse the distance, h, can be estimated as $T_D = h^2 / D$. For a ciliate like *V. convallaria* with $h = 100 \ \mu\mathrm{m}$ this corresponds to $T_D = 14$ h for nonmotile prey and $T_D = 6$ min for motile prey. The timescale for nonmotile prey is fairly long, whereas the timescale for motile prey is short compared to the shortest recirculation time in the representative example, suggesting that diffusion makes recirculation irrelevant in perpendicular feeding flow with motile prey. The effect of motility on recirculation is presumably even more significant for motile prey with long run length that move ballistically on the length scale of the clearance zone, and for such prey types motility may furthermore significantly enhance the transport toward the clearance zone [34].

Marine snow particles and other habitats for attached suspension feeders typically have some regions that are shielded from ambient flow while others are exposed. To estimate the possible effects of ambient flow close to a typical marine snow particle, we consider a spherical particle with radius $R = 2$ mm and sinking speed $U = 0.9$ mm s^{-1} [14]. The Reynolds number for such a particle

TABLE I. Parameters for the choanoflagellate *S. rosetta* and the ciliate *V. convallaria* (Fig. 1). The equivalent spherical radius of the cell, ESR, the height above the surface, h, the height, d, and the radius, a, of the clearance disk, the magnitude of the flow-generating force, F, and the timescale T_0 obtained using Eq. (6) with $\mu = 1 \times 10^{-3}$ Pas.

Species	ESR (μm)	h (μm)	d (μm)	a (μm)	F (pN)	T_0 (s)	Source
S. rosetta	2	17	7–13	3	2	4	[10,12]
V. convallaria	16	100	100	15	50–500	0.5–5	[9]

is on the order of unity, but for simplicity we assume low-Reynolds-number flow. Close above the surface, the magnitude of the parallel velocity component, u, increases linearly with the height above the surface, δ, whereas the magnitude of the perpendicular velocity component increases quadratically. The parallel flow vanishes at the poles of the spherical particle, and it is largest at the equator:

$$u \approx \frac{3\delta U}{2R}.$$

(27)

The clearance rate of a parallel feeder may be either enhanced or reduced depending on its orientation relative to the ambient flow. As an example of a parallel feeder we consider the ciliate *Euplotes moebiusi* with $h = 30$–34 μm and typical feeding flow speeds of approximately 300–400 μm s^{-1} ([5], Table 2 and Fig. 29). With $\delta = 34$ μm we estimate the ambient flow speed $u = 23$ μm s^{-1}, suggesting that ambient flow is an order of magnitude weaker than the self-generated feeding flow. To lowest order, the flow through the clearance disk of a perpendicular feeder will not be affected directly by the predominantly parallel ambient flow. However, since perpendicular feeders are positioned relatively high above the surface, they will experience stronger ambient flow than their parallel counterparts. Such ambient flow might disrupt the recirculating streamline pattern and influence both orientation and height of organisms with thin stalks such as *V. convallaria*.

VII. CONCLUSIONS

Quantitative experimental data for near field flows and prey capture in sessile suspension feeders are sparse, and additional quantitative observations of feeding flows, clearance zone geometries, and recirculation times for representative flagellates and ciliates would complement the extensive data on morphological characteristics that exists in the literature. Such observations will allow predictions based on the point force model and open for quantitative explorations of its applicability, while the testable hypotheses discussed in the present paper will provide valuable inspiration for the analysis of the observations.

ACKNOWLEDGMENTS

[1] G. Lapage, Notes on the Choanoflagellate, *Codosiga botrytis*, Ehrbg. Q. J. Microsc. Sci. **69**, 471 (1925).

[2] M. A. Sleigh and D. Barlow, Collection of food by *Vorticella*, Trans. Am. Microsc. Soc. **95**, 482 (1976).

[3] J. J. L. Higdon, The generation of feeding currents by flagellar motion, J. Fluid Mech. **94**, 305 (1979).

[4] T. Fenchel, Suspension feeding in ciliated protozoa—Structure and function of feeding organelles, Arch. Protist. **123**, 239 (1980).

[5] T. Fenchel, Protozoan filter feeding, Prog. Protistol. **1**, 65 (1986).

[6] J. R. Blake and S. R. Otto, Ciliary propulsion, chaotic filtration and a 'blinking' stokeslet, J. Eng. Math. **30**, 151 (1996).

[7] K. K. Christensen-Dalsgaard and T. Fenchel, Increased filtration efficiency of attached compared to free-swimming flagellates, Aquat. Microb. Ecol. **33**, 77 (2003).

[8] R. E. Pepper, M. Roper, S. Ryu, P. Matsudaira, and H. A. Stone, Nearby boundaries create eddies near microscopic filter feeders, J. R. Soc. Interface **7**, 851 (2010).

[9] R. E. Pepper, M. Roper, S. Rye, N. Matsumoto, M. Nagai, and H. A. Stone, A new angle on microscopic suspension feeders near boundaries, Biophys. J. **105**, 1796 (2013).

[10] M. Roper, M. J. Dayel, R. E. Pepper, and M. A. R. Koehl, Cooperatively Generated Stresslet Flows Supply Fresh Fluid to Multicellular Choanoflagellate Colonies, Phys. Rev. Lett. **110**, 228104 (2013).

[11] J. B. Kirkegaard and R. E. Goldstein, Filter-feeding, near-field flows, and the morphologies of colonial choanoflagellates, Phys. Rev. E **94**, 052401 (2016).

[12] H. Nguyen, M. A. R. Koehl, C. Oakes, G. Bustamante, and L. Fauci, Effects of cell morphology and attachment to a surface on the hydrodynamic performance of unicellular choanoflagellates, J. R. Soc. Interface **16**, 20180736 (2019).

[13] M. J. Dayel, Choanoflagellates and animal multicellularity, Scanning electron micrograph of *S. rosetta* thecate cell licensed under the creative commons share-alike license, http://www.dayel.com/choanoflagellates/.

[14] A. L. Alldredge and C. Gotschalk, In situ settling behavior of marine snow, Limnol. Oceanogr. **33**, 339 (1988).

[15] T. Kiørboe and G. A. Jackson, Marine snow, organic solute plumes, and optimal chemosensory behavior of bacteria, Limnol. Oceanogr. **46**, 1309 (2001).

[16] J. R. Seymour, Marcos, and R. Stocker, Resource patch formation and exploitation throughout the marine microbial food web. Am. Nat. **173**, E15 (2009).

[17] S. Smriga, V. I. Fernandez, J. G. Mitchell, and R. Stocker, Chemotaxis toward phytoplankton drives organic matter partitioning among marine bacteria, Proc. Natl. Acad. Sci. USA **113**, 1576 (2016).

[18] K. Malmcrona-Friberg, B. L. Blainey, and K. C. Marshall, Chemotactic response of a marine bacterium to breakdown products of an insoluble substrate, FEMS Microbiol. Lett. **85**, 199 (1991).

[19] A. L. Alldredge and M. W. Silver, Characteristics, dynamics and significance of marine snow, Prog. Oceanogr. **20**, 41 (1988).

[20] T. Kiørboe, Marine snow microbial communities: Scaling of abundances with aggregate size, Aquat. Microb. Ecol. **33**, 67 (2003).

[21] T. Kiørboe, K. Tang, H.-P. Grossart, and H. Ploug, Dynamics of microbial communities on marine snow aggregates: Colonization, growth, detachment, and grazing mortality of attached bacteria, Appl. Environ. Microbiol. **69**, 3036 (2003).

[22] H. C. Berg, *Random Walks in Biology* (Princeton University Press, Princeton, NJ, 1993).

[23] J. R. Blake, A note on the image system for a stokeslet in a no-slip boundary, Math. Proc. Cambr. Philos. Soc. **70**, 303 (1971).

[24] J. R. Blake and A. T. Chwang, Fundamental singularities of viscous flow, J. Eng. Math. **8**, 23 (1974).

[25] K. Aderogba and J. R. Blake, Action of a force near the planar surface between semi-infinite immiscible liquids at very low Reynolds numbers: Addendum, Bull. Aust. Math. Soc. **19**, 309 (1978).

[26] N. Liron, Fluid transport by cilia between parallel plates, J. Fluid Mech. **86**, 705 (1978).

[27] N. Liron and J. R. Blake, Existence of viscous eddies near boundaries, J. Fluid Mech. **107**, 109 (1981).

[28] G. K. Batchelor, *An Introduction to Fluid Dynamics* (Cambridge University Press, Cambridge, UK, 1967).

[29] J. D. Lawrence, *A Catalog of Special Plane Curves* (Dover, London, 1972).

[30] S. H. Strogatz, *Nonlinear Dynamics and Chaos: With Applications to Physics, Biology, Chemistry, and Engineering*, 2nd ed. (Westview Press, Boulder, CO, 2015).

[31] A. W. Visser and T. Kiørboe, Plankton motility patterns and encounter rates, Oecologia **148**, 538 (2006).

[32] J. E. Johansen, J. Pinhassi, N. Blackburn, U. L. Zweifel, and Å. Hagström, Variability in motility characteristics among marine bacteria, Aquat. Microb. Ecol. **28**, 229 (2002).

[33] J. Dölger, L. T. Nielsen, T. Kiørboe, and A. Andersen, Swimming and feeding of mixotrophic biflagellates, Sci. Rep. **7**, 39892 (2017).

[34] V. J. Langlois, A. Andersen, T. Bohr, A. W. Visser, and T. Kiørboe, Significance of swimming and feeding currents for nutrient uptake in osmotrophic and interception-feeding flagellates, Aquat. Microb. Ecol. **54**, 35 (2009).